CoFe2O4 and CoFe2O4/SiO2 Core/Shell nanoparticles: magnetic and spectroscopic study. Chem Mater

ARTICLE *in* CHEMISTRY OF MATERIALS · JUNE 2010

Impact Factor: 8.35 · DOI: 10.1021/cm903837g

CHEMISTRY OF MATERIALS
Article

Chem. Mater. **2010,** *22,* 3353–3361 3353
DOI:10.1021/cm903837g

$CoFe_2O_4$ and $CoFe_2O_4/SiO_2$ Core/Shell Nanoparticles: Magnetic and Spectroscopic Study

Carla Cannas,*,† Anna Musinu,† Andrea Ardu,† Federica Orrù,† Davide Peddis,† Mariano Casu,† Roberta Sanna,† Fabrizio Angius,‡ Giacomo Diaz,‡ and Giorgio Piccaluga†

†*Dipartimento di Scienze Chimiche, Università di Cagliari, Cittadella Universitaria, 09042, Monserrato (Cagliari), Italy, and* ‡*Dipartimento di Scienze e Tecnologie Biomediche Sezione di Patologia Sperimentale via Porcell, 4 - 09100 Cagliari (CA), Italy*

Received December 23, 2009. Revised Manuscript Received March 23, 2010

Spherical nanoparticles of surfactant-coated $CoFe_2O_4$ (core) were prepared through thermal decomposition of metal acetylacetonates in the presence of a mixture of oleic acid and oleylamine and uniformly coated with silica shell by using tetraethylorthosilicate (TEOS) and ammonia in a micellar solution (core/shell). Transmission electron microscopy (TEM) analysis of core/shell nanoparticles evidenced the high homogeneity of the coating process in producing single core/shell nanoparticles with a narrow size distribution. The combined use of spectroscopic studies (NMR and FTIR) on core and core/shell nanoparticles pointed out that the surfactants' layer bound to the surface core nanoparticles is retained also after the silica coating process. This allows to obtaining systems with very similar magnetic behavior but weaker dipolar interparticle interactions and lower values of saturation magnetization. In view of the interest in biomedical field, the effect of the $CoFe_2O_4$ nanoparticles silica coating was also studied by controlling the possible modifications in cytotoxicity by trypan blue and 3-(4,5-dimethylthiazol-2-yl)-2,5-diphenyltetrazoliumbromide (MTT) assays on human cells.

Introduction

The use of magnetic nanoparticles for biomedical purposes has been proposed to a large extent in recent years.[1−4] This kind of application requires that the surface of the nanoparticles be modified both for protection and functionalization needs.[5,6] This is particularly important in the case of cobalt ferrites nanoparticles. $CoFe_2O_4$ is in fact very attractive in the biomedical field for its high magnetic anisotropy and saturation magnetization which give rise to suitable magnetic behavior at room temperature, but the presence of cobalt makes it potentially toxic.[7,8]

To protect magnetic nanoparticles, encapsulation both in polymeric and inorganic matrixes has been proposed,[9] but silica has been most often used.[10−12] This is why SiO_2 provides coating shells that are stable, nontoxic, hydrophilic, and biocompatible, and in addition, it can be easily functionalized to bind biomolecules on its surface silanolic groups.

However, it has been reported that the shell of SiO_2 can alter the properties of the magnetic coated core.[13] This can be ascribed to the modification of interparticles interactions, to the arising of novel properties in confined nanoparticles and, more probably, to the surface effects at the core/shell contact. In particular, this effect has been observed in Mn and Co spinel ferrite-silica nanoparticles.[14] In this case the modification of magnetic properties (for instance, coercivity) was greater in $MnFe_2O_4$ than in $CoFe_2O_4$, presumably because the high magnetocrystalline anisotropy of cobalt ferrite diminishes the importance of the contribution of surface anisotropy to the total anisotropy and its variation upon coating.

The present paper examines the effects on magnetic properties of $CoFe_2O_4$ nanoparticles induced by their coating with SiO_2. Among the many methods proposed for the nanoferrites' preparation (precipitation from

*Corresponding author. E-mail:ccannas@unica.it.

(1) Pankhurst, Q. A.; Connolly, J.; Jones, S. K.; Dobson, J. *J. Phys. D, Appl. Phys.* **2003**, *36*, R167.
(2) Pankhurst, Q. A.; Thanh, N. K. T.; Jones, S. K.; Dobson, J. *J. Phys. D, Appl. Phys.* **2009**, *42*, 224001.
(3) Gupta, A. K.; Gupta, M. *Biomaterials* **2005**, *26*, 3995.
(4) Roca, A. G.; Costo, R.; Rebolledo, A. F.; Veintemillas-Verdaguer, S.; Tartaj, P.; Gonzalez-Carreno, T.; Morales, M. P.; Serna, C. J. *J. Phys. D: Appl. Phys.* **2009**, *42*, 224002.
(5) Berry, C. C.; Curtis, A. S. G. *J. Phys. D, Appl. Phys.* **2003**, *36*, R198.
(6) Berry, C. C. *J. Phys. D: Appl. Phys.* **2009**, *42*, 224003.
(7) Kuckelhaus, S.; Reis, S. C.; Carneiro, M. F.; Tedesco, A. C.; Oliveira, D. M.; Lima, E. C. D.; Morais, P. C.; Azevedo, R. B.; Lacava, Z. G. M. *J. Magn. Magn. Mater.* **2004**, *272*, 2402.
(8) Baldi, G.; Bonacchi, D.; Innocenti, C.; Lorenzi, G.; Sangregorio, C. *J. Magn. Magn. Mater.* **2007**, *311*, 10.
(9) Tartaj, P.; Del Puerto Morales, M.; Veintemillas-Verdaguer, S.; Gonzalez-Carreno, T.; Serna, C. J. *J. Phys. D, Appl. Phys.* **2003**, *36*, R182.
(10) Lin, Y. S.; Haynes, C. L. *Chem. Mater.* **2009**, *21*, 3979.
(11) Yi, D. K.; Lee, S. S.; Papaefthymiou, C. G.; Ying, J. Y. *Chem. Mater.* **2006**, *18*, 614.
(12) Lin, Y. S.; Haynes, C. L. *Chem. Mater.* **2009**, *21*, 3979.
(13) Fang, H.; Ma, C.; Wa, T.; Zhang, M.; Shi, W. *J. Phys. Chem. C* **2007**, *111*, 1065.
(14) Vestal, C. R.; Zhang, Z. J. *Nano Lett.* **2003**, *3*, 1739.

Published on Web 04/30/2010

solutions, microemulsion, polyols, aerosol-vapor methods, spray pyrolysis, laser pyrolysis, hydrothermal methods, high-temperature decomposition of organic precursors),[9,15−17] we adopted the one described by Sun et al.[18] that makes use of a solution reaction of metals acetylacetonates with 1,2-hexadecanediol in the presence of a mixture of oleic acid and oleylamine. This route is particularly advantageous as regards the distribution and tunability of sizes, the high degree of crystallinity, and the moderate treatment temperature. Furthermore, it provides particles that are presumably covered by a stable and difficult to remove oleic coating. This shell has been considered responsible for the reduction of dipolar interparticles interactions and surface spin canting.[18] In the hypothesis that the coating process does not remove the surfactant envelopment, the silica shell should not modify sensibly the magnetic properties of the core; in this case, "core" obviously indicates the inorganic particle plus its surfactant coating.

To coat core nanoparticles with silica we used a micellar−sol−gel combined route. The procedure has been recently proposed by Vestal and Zhang,[14] who experienced it on particles prepared through micellar procedures that did not make use of oleic acid and oleylamine. The same procedure has been applied by Zhang et al.[19] on magnetite nanoparticles coming from the acetylacetonate route, but in this work, no comparison was made between the magnetic properties of the Fe_3O_4 core and Fe_3O_4/SiO_2 core/shell particles.

In the quoted literature, the state of oleic acid and oleylamine in the core and core/shell nanoparticles was not investigated. Therefore, the present paper reports a comparative magnetic and spectroscopic study. To this end, besides FTIR spectra, we collected ^{1}H NMR spectra of the ligands bonded to the superparamagnetic nanocrystals, according to the nonconventional approach of Willis et al.[20] In view of the interest in the biomedical field, the effect of the $CoFe_2O_4$ nanoparticles silica coating was also studied by controlling the possible modifications in cytotoxicity. Cytotoxicity was evaluated on human cells by trypan blue and 3-(4,5-dimethylthiazol-2-yl)-2,5-diphenyltetrazoliumbromide (MTT) assays.[11,21,22]

Experimental Section

Core: $CoFe_2O_4$ Nanoparticles Preparation. $CoFe_2O_4$ nanoparticles were prepared by following the procedure described in ref 18. To synthesize $CoFe_2O_4$ nanoparticles of about 8 nm, iron(III) acetylacetonate (Janssen Chimica 99%, 2 mmol), cobalt(II) acetylacetonate (Janssen Chimica 99%, 1 mmol), 1,2-hexadecanediol (Aldrich 97%, 10 mmol), oleic acid (Aldrich 90%, 6 mmol), oleylamine (Aldrich $<70\%$, 6 mmol), and benzylether (Aldrich 99%, 20 mL) were mixed into a three-neck, round-bottom flask and stirred magnetically. Under reflux, the mixture was heated gradually to 200 °C and kept at this temperature for 2 h. The temperature was then increased rapidly up to 300 °C, and the mixture kept for 1 h at this temperature. The black-colored mixture was cooled to room temperature by removing the heat source. Ethanol (about 40 mL) was then added to the mixture and the black material was precipitated and separated via centrifugation. The product was then dispersed in hexane or in cyclohexane and centrifugated once more to remove any undispersed residue, giving rise to a ferrofluid that retains its stability for several months. The nanoparticles were precipitated through the addition of a large amount of ethanol, separated by centrifugation, and dried at 40 °C overnight to evaporate alcohol residual.

Core/Shell: $CoFe_2O_4$/Silica Nanoparticles Preparation. Silica coating of $CoFe_2O_4$ nanoparticles was performed through the formation of microemulsions based on the base-catalyzed hydrolysis of tetraethylorthosilicate (TEOS).[14,19] Specifically, in order to achieve a 10−12 nm thick silica shell, 0.56 mmol of the nonionic surfactant polyoxyethylene(5)nonylphenyl ether (IGEPAL CO-520, Aldrich) was dispersed in 4 mL of cyclohexane by sonication. Then, 300 μL of $CoFe_2O_4$ ferrofluid (0.8 mg/mL ciclohexane), previously sonicated for a few minutes, was added, and the mixture was vigorously stirred at room temperature for 15 min. TEOS (Aldrich 98%, 20 μL) was added, the resulting mixture stirred for 30 min, and then liquor ammonia (Aldrich 30%, 35 μL) was added. The reaction was allowed to proceed at room temperature for 24 h under stirring.

The core/shell nanoparticles were destabilized from the microemulsion by using methanol and precipitated by centrifugation. The resultant precipitate was washed in sequence with methanol and water to remove any possible surfactant and unreacted molecules. For each washing step, followed by centrigugation, a sonicator bath was used to completely disperse the precipitate in the corresponding solvent and to remove any physically adsorbed molecule from the particle surface. Finally, the wet powder was dried at 60 °C overnight.

Characterization Techniques. Finely ground samples were dispersed in octane and submitted to an ultrasonic bath. The suspensions were then dropped on carbon-coated copper grids for the TEM observations. Cobalt−ferrite nanoparticles were observed in electron micrographs obtained with a TEM (JEOL 200CX), operating at 200 kV.

DC magnetization measurements were performed with a Quantum Design SQUID magnetometer, equipped with a superconducting coil which produces magnetic fields in the range from −5 to +5 T.

The samples in the form of powders were immobilized in an epoxy resin to prevent any movement of the nanoparticles during the measurements.

Magnetization versus temperature measurements were performed using the zero field cooled (ZFC), field cooled (FC), and thermoremanent magnetization (TRM) protocols. Zero field cooled and field cooled magnetization measurements were carried out by cooling the sample from room temperature to 5 K in zero magnetic field; then, a static magnetic field of 2.5 mT was applied. M_{ZFC} was measured during warming from 5 to 300 K, whereas M_{FC} was recorded during the subsequent cooling. In the TRM measurements, the sample was cooled from 300 to 5 K in an external magnetic field of 2.5 mT; then, the

(15) Mathew, D. S.; Juang, R. S. *Chem. Eng. J.* **2007**, *129*, 51.
(16) Bao, N.; Shen, L.; An, W.; Padhan, P.; Turner, C. H; Gupta, A. *Chem. Mater.* **2009**, *21*, 3458.
(17) Suber, L.; Peddis, D. Approaches to synthesis and characterization of spherical and anisometric metal oxide magnetic nanomaterials. In *Magnetic Nanomaterial*; Kumar, C., Ed.; Wiley: New York, 2009
(18) Sun, S.; Zeng, H.; Robinson, D. B.; Raoux, S.; Rice, P. M.; Wang, S. X.; Li, G. *J. Am. Chem. Soc.* **2004**, *126*, 273.
(19) Zhang, M. B.; Cushing, L.; O'Connor, C. J. *Nanotechnology* **2008**, *19*, 85601.
(20) Willis, A. L.; Turro, N. J.; O'Brien, S. *Chem. Mater.* **2005**, *17*, 5970.
(21) Bihari, P.; Vippola, M.; Schultes, S.; Praetner, M.; Khandoga, A. G.; Reichel, C. R.; Coester, T.; Rehberg, M.; Krombach, F. *Part. Fibre Toxicol.* **2008**, *5*(14), 1.
(22) Tomitaka, A.; Hirukawa, A.; Yamada, T.; Morishita, S.; Takemura, Y. *J. Magn. Magn. Mater.* **2009**, *321*, 1482.

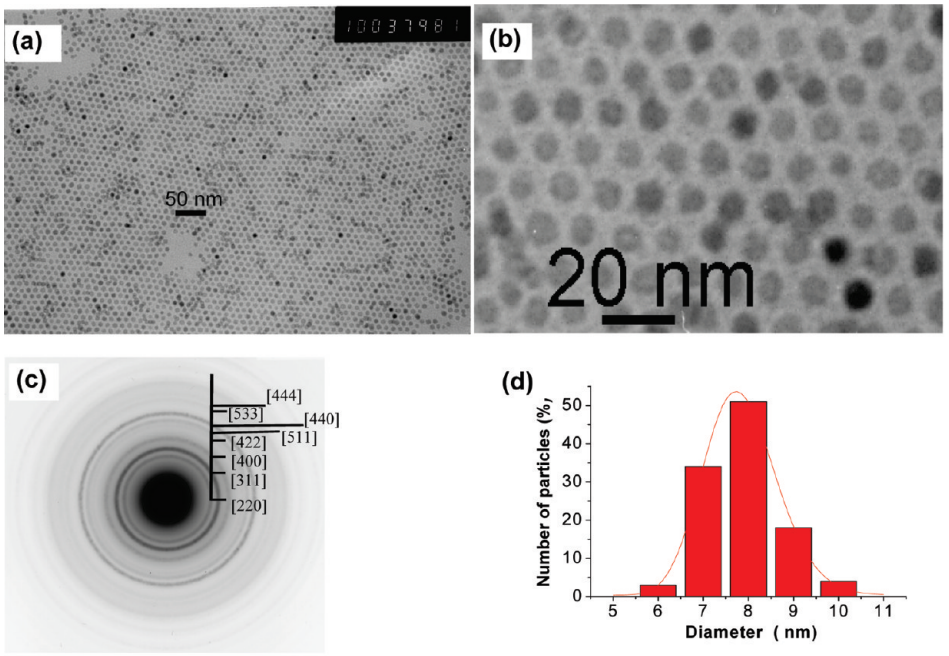

Figure 1. TEM data of $CoFe_2O_4$ core nanoparticles. (a) Bright field image at low magnification. (b) Detail of a. (c) Selected area diffraction. (d) Particle size distribution.

field was turned off and magnetization was measured on warming up.

The field dependence of remanent magnetization was measured using the IRM (isothermal remanent magnetization) and DCD (direct current demagnetization) protocols.

The initial state for an IRM measurement is a totally demagnetized sample cooled in a zero magnetic field. In the present case, an external field was applied for 10 s, then it was switched off and the remanence was measured (M_{IRM}). The process was repeated, increasing the field until saturation. In a DCD measurement, the initial state is the magnetically saturated one. An external field of -5 T was applied for 10 s, then a small external field in the direction opposite to magnetization was applied, and, after 10 s, it was switched off and the remanent magnetization (M_{DCD}) was measured. This was repeated increasing the field up to $+5$ T.[23]

^{1}H NMR spectra of the core and core/shell nanoparticles dispersed in $CDCl_3$ were collected on a Varian Unity-Inova spectrometer at a resonance frequency of 399.948 MHz and at $T = 28 \pm 0.1$ °C. The experiments were carried out on a 5 mm tube using 7 μs pulse (90°), 1 s repetition time, and spectral width of 10 kHz. Chemical shifts in all the spectra are referenced to DSS (2,2-dimethyl-2-silapentane-5-sulfonate) through the residual solvent signal.

FTIR spectra were collected in the region from 400 to 3800 cm^{-1}, using a Bruker Equinox 55 spectrophotomer. Surfactants were analyzed by placing a drop of the liquid between KBr windows, while core and core/shell powders were dispersed in KBr pellets.

Cytotoxicity Assays. Cytotoxicity of the nanoparticles was screened in CCRF-CEM (human T cell leukemia) cells (ATCC, Rockville, MD). Cells were diluted, allowed to grow for 24 h, and then incubated with suitable water or fetal calf serum (FCS)[21] nanoparticles dispersions. Nanoparticles were dispersed in water or FCS at 100-fold concentrations with respect to the final concentration in the medium. Thereafter, the dispersions were immediately added after sonication to the culture medium in the 1:100 ratio to obtain the final nanoparticle concentrations of 20 μg/mL for $CoFe_2O_4$ and 100 μg/mL for $CoFe_2O_4-SiO_2$. The presence of 10% serum in the medium should have blocked the spontaneous agglomeration of nanoparticles observed in neutral physiological saline solution.[21] Durations of treatments were 0 (baseline), 24, 48, and 72 h. At each time point and for each treatment, the number of viable cells was determined with a Bürker chamber by trypan blue (TB) dye exclusion in duplicate. Cell viability was also determined by the 3-(4,5-dimethylthiazol-2-yl)-2,5-diphenyltetrazoliumbromide (MTT) assay. Further details are reported in the Supporting Information.

Results

Characterization. TEM analysis shows the formation of essentially spherical and uniform nanoparticles (Figure 1a and b); electron diffraction (Figure 1c) reveals that the core oxide particles are crystallized in the $CoFe_2O_4$ phase. These nanoparticles self-assemble in hexagonal close-packed superlattice, due to the high degree of uniformity in diameter (Figure 1b). The presence of the residual surfactants at the nanoparticle surface keeps them isolated from each other by a coating layer of about 2 nm, giving rise to an ideal system for the next step of coating with silica. Particle size distribution, calculated on about 200 nanoparticles in different images in bright field mode and fitted with a log-normal distribution, leads to a measured mean diameter of 7.8 nm and a polidispersity of 10% (Figure 1d). The crystalline phase and particle size are consistent with that obtained by XRD, which shows crystalline reflexes corresponding to a unique cubic $CoFe_2O_4$ phase (pdf card N 22-1086; Supporting Information).

Silica coated nanoparticles were examined by TEM, and two images of a sample before drying are here

(23) O'Grady, K.; Chantrell, R. W. Proceding of the International workshop on Studies of Magnetic Properties of Fine Particles and their relevance to Materials Science; **1992**.

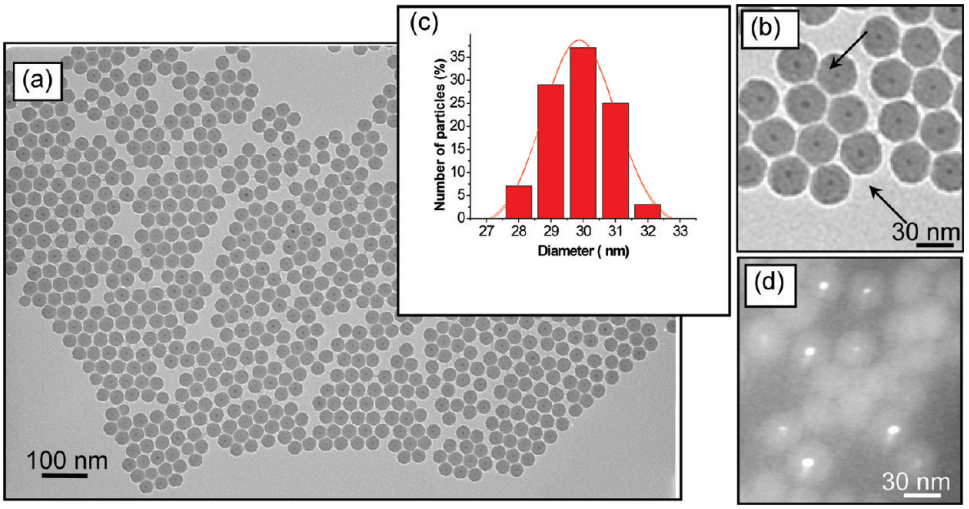

Figure 2. TEM data of $CoFe_2O_4-SiO_2$ core/shell nanoparticles. (a) Bright field image at low magnification. (b) Detail of a. (c) Particle size distribution. (d) Dark field image.

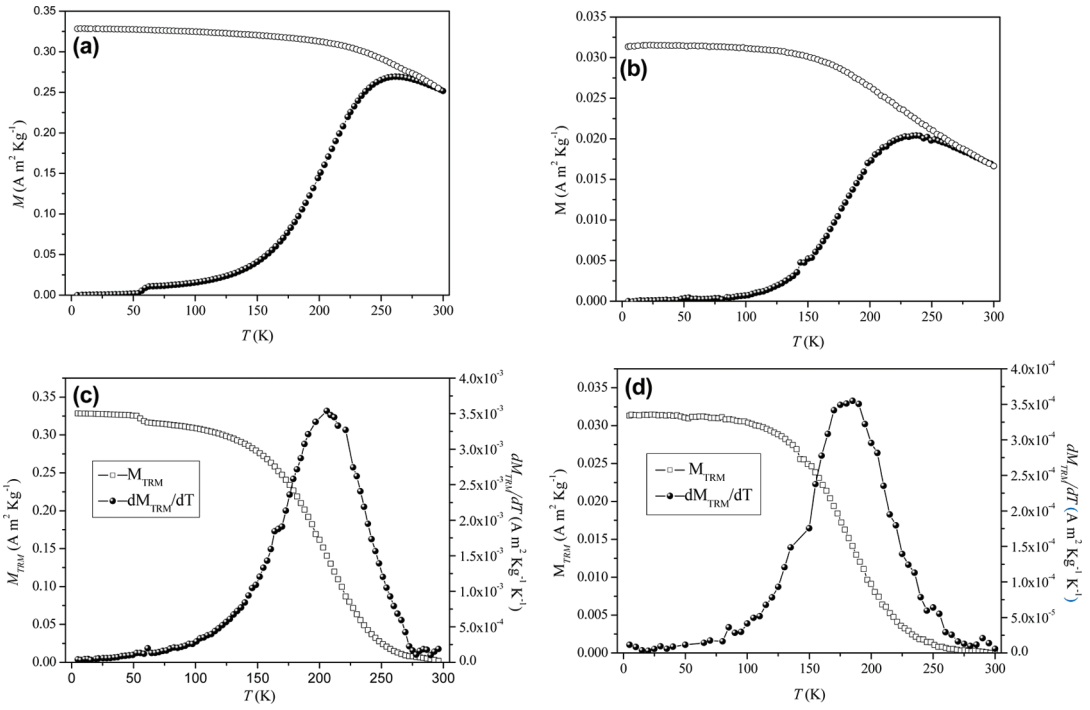

Figure 3. (upper part) ZFC (full symbols) and FC (empty symbols) curves for the $CoFe_2O_4$ core (a) and $CoFe_2O_4-SiO_2$ core/shell samples (b). (lower part) TRM (empty symbols) and distribution of magnetic anisotropy (full symbols) for the core (c) and core/shell samples (d).

reported as an example (Figure 2a and b). TEM images in bright field mode show the formation of spherical core/shell structures with an average overall size of 30 nm and a polidispersity of 5% (Figure 2c) with a single magnetic core in the center of the spheres. The TEM image in dark field mode (Figure 2d) confirms the high degree of crystallinity of the core and the amorphous nature of the shell, that was also observed by XRD (Supporting Information). The assembling of the nanoparticles appears to be in the form of hexagonal close packing. In some cases a deviation from spherical shape can be observed (Figure 2b); this can be due to a slight deformation of the particles along the close packing direction.

Figure 3a and b show ZFC and FC magnetization curves for the core and the core/shell samples, respectively. The samples show a qualitatively similar behavior. ZFC curves exhibit a maximum, and the corresponding temperature (T_{max}) is directly proportional to the average blocking temperature.[24] An irreversible magnetic behavior is observed below a given temperature (T_{irr}) that is related to the blocking of the biggest particles. The difference between T_{max} and T_{irr} provides a qualitative measure of the magnetic anisotropy distribution, which is strictly connected with the size distribution in the absence of interparticle interactions.[25] Going to lower temperatures, the FC curves show a temperature-independent behavior, indicating the presence of a magnetic ordered state with

(24) Gittleman, J. I.; Abeles, B.; Bozowski, S. *Phys. Rev. B* **1974**, *9*, 389.
(25) Hansen, M. F.; Mørup, S. *J. Magn. Magn. Mater.* **1999**, *203*, 214.

Table 1. Mean Particle Size from TEM data ($< D_{TEM} >$), Temperature Corresponding to the Maximum in ZFC Curve (T_{max}), Irreversibility Temperature (T_{irr}), Difference between T_{irr}, and T_{max} ($T_{irr} - T_{max}$), Blocking Temperature from TRM Measurement (T_B), Coercivity (H_c), and Reduced Remanent Magnetization (M_r/M_s) at 5 K

sample	$< D_{TEM} >$ (nm)	σ %	T_{max} (K)	T_{irr} (K)	$(T_{irr} - T_{max})$ (K)	T_B (K)	H_c (5 K) (T)	M_r/M_s (5 K)
core	7.8	10	262(5)	283(4)	21(2)	200(4)	1.71 (2)	0.88(2)
core/shell	30	5	235(5)	254(4)	19(2)	181 (3)	1.98 (1)	0.90(2)

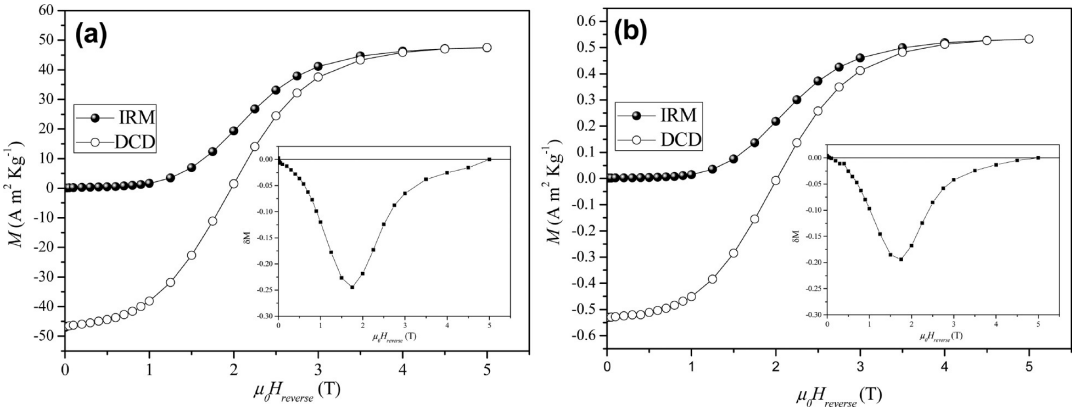

Figure 4. DCD and IRM curves for core (a) and core/shell samples (b). The insets show δM plat for core (a) and core shell (b) samples.

high anisotropy.[26,27] The quantitative comparison between T_{max}, T_{irrr}, and $(T_{irr} - T_{max})$ values (Table 1) gives some indications regarding the differences between the two samples.

$(T_{irr} - T_{max})$ values are equal within the experimental error, confirming that the two samples are similar in the distribution of magnetic anisotropy. On the other hand, T_{irr} and T_{max} clearly decrease in the core/shell sample. Considering that mean particle size, magnetic anisotropy distribution, and magnetocrystalline anisotropy are similar, this behavior can be ascribable to a decrease of interparticle interactions due to the presence of a silica shell.

Figure 3c and d shows measurements of the magnetization as a function of temperature, carried out with the TRM procedure (empty symbols) for core and core/shell samples, respectively. For both samples, M_{TRM} decreases with increasing temperature, as can be expected for an assembly of magnetic monodomain particles. For noninteracting particles, the derivative of M_{TRM} with respect to temperature gives an estimate of the anisotropy energy barrier distribution,

$$f(\Delta E_a) \propto -\frac{dM_{TRM}}{dT} \quad (1)$$

In our samples, the derivative of M_{TRM} can actually be considered only as an indication of the ΔE_a distribution, seeing that the role of the interparticle interactions on physical behavior of both samples cannot be disregarded.

Figure 3c and d show the ΔE_a distribution (full symbols) for core and core/shell nanoparticles, respectively. Within the Néel model, the blocking temperature (T_B) can be defined as the temperature for which the relaxation time is equal to the measuring time of the experimental technique. In practice, samples of small particles always exhibit particle size distributions, and often T_B is defined as the temperature at which 50% of the sample is in the superparamagnetic state. We can obtain an estimate of the blocking temperature from the distribution of the magnetic anisotropy energy barriers by evaluating the temperature at which 50% of the particles overcome their anisotropy energy barriers. In Table 1, the values of the blocking temperature T_B obtained with this method are reported. T_B values follow the same trend of T_{max} and T_{irr}, confirming a decrease of interparticle interactions due to the presence of silica shell.

The dependence of magnetization on an external magnetic field was studied at 5 K. An increase of coercivity (H_c, Table 1) is observed in core shell particles, ascribable to the decrease of interparticle interactions.[28,29] For both samples, the reduced remanent magnetization (M_r/M_s, Table 1) suggests the presence of cubic magnetocrystalline anisotropy.

In order to gain a deeper insight into interparticle interactions, the dependence of remanent magnetization on the field was analyzed at 5 K, according to isothermal remanent magnetization (IRM) and remanent magnetization after direct current demagnetization (DCD) protocols. DCD and IRM curves are reported in Figure 4a and b for core and core/shell samples.

In a noninteracting assembly of nanoparticles with uniaxial anisotropy, the same energy barrier distribution should be determined from M_{IRM} and M_{DCD}, as is clearly expressed from the Wohlfart relation:

$$M_{DCD}(H) = 1 - 2M_{IRM}(H) \quad (2)$$

(26) Cannas, C.; Ardu, A.; Musinu, A.; Peddis, D.; Piccaluga, G. *Chem. Mater.* **2008**, *20*, 6364.
(27) Kelly, P. E.; Grady, K. O.; Mayo, P. I.; Chantrell, R. W. *IEEE Trans. Magn.* **1989**, *25*, 3881.
(28) El-Hilo, M.; Chantrell, R. W.; O'Grady, K. *J. Appl. Phys.* **1998**, *84*, 5114.
(29) Cannas, C.; Falqui, A.; Musinu, A.; Peddis, D.; Piccaluga, G. *J. Nanopart. Res.* **2006**, *8*, 255.

Kelly et al.[27] rewrote the Wohlfart relation to explicitly reveal deviations from a noninteracting case

$$\delta M = M_{DCD} - [1 - 2M_{IRM}(H)] \quad (3)$$

Negative δM are usually taken as indicative of the presence of interactions that have the effect of stabilizing the demagnetized state (i.e., dipole−dipole interactions). Positive values of δM are usually attributed to interactions promoting the magnetized state (i.e., exchange interactions).

The conclusions of this procedure regarding particles with cubic anisotropy have to be taken with care. Indeed δM plots, calculated for the case of randomly oriented noninteracting particles with cubic anisotropy, deviate from linearity toward "positive" values.[30,31] On the other hand, the remanence curve technique (defined for systems of uniaxial anisotropy) has been often applied, without any modification to systems consisting of particles with mixed multiaxial and uniaxial anisotropy.[32] In our case, δM plots are negative and this clearly indicates the prevalence of demagnetizing dipolar interactions in both samples.

The prevalence of dipolar interactions confirms the morphological features evidenced by TEM: oleic and silica coatings are homogeneous in core and core/shell samples, respectively, preventing any kind of aggregations among nanoparticles.

A semiquantitative evaluation of interparticle interactions can be made using the so-called coercivity factor (CF)[30]

$$CF = \left(\frac{H_r}{H_c} - 1\right) \times 100 \quad (4)$$

where H_r is the remanence coercivity (Table 1), defined as the reverse field corresponding to $M_{DCD} = 0$.

CF values for core and core/shell samples are respectively 18% and 2%. This confirms the key role of the silica shell in the decrease of the dipolar interactions, due to the increase of the interparticles distance. The decrease of interparticle interactions is corroborated by evaluating the magnetic dipolar energy assuming a point-dipole model[33] (i.e., center to center minimum distance) which gives E_{dip}/k_B equal to about 60 and 4 K for core and core/shell samples, respectively. For both samples, E_{dip}/k_B is lower than T_B, indicating that the transition ferromagnetic−superparamagnetic is mainly governed by magnetic anisotropy energy of the nanoparticles. However, it should be pointed out that for the core sample interparticle interaction can influence the magnetic behavior of the nanoparticles.

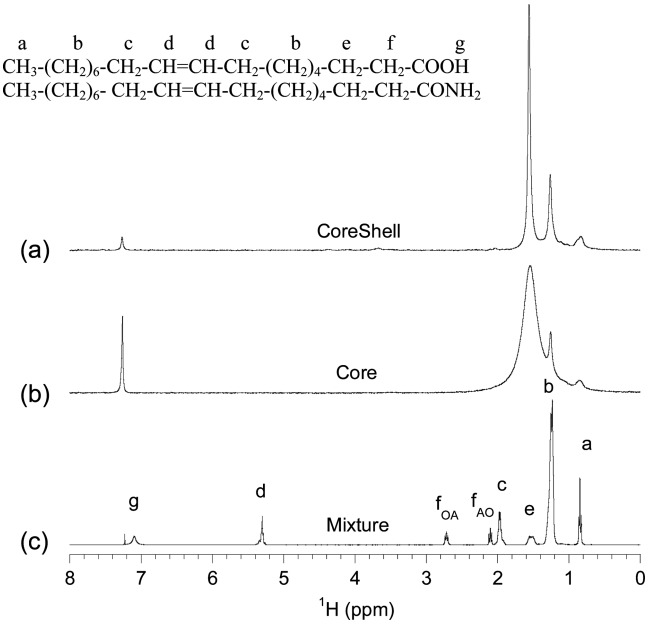

Figure 5. ^{1}H NMR spectra of (a) core/shell nanoparticles, (b) core, and (c) the mixture of the surfactants (1:1 mixture of oleic acid and oleylamine). fOA (Oleylamine); fAO (Oleic acid).

Solution ^{1}H NMR spectroscopy has become a very useful tool in investigating the ligands bound to the surface of diamagnetic nanoparticles.[34−36] The study of ligands on magnetic nanoparticles by ^{1}H NMR is rarely performed. In fact, the presence of paramagnetic metals can influence the chemical shift, the spin−lattice relaxation rates, and the line width of the proton signals.[37] The spectra can show remarkable differences, and resonances in a large volume sphere around the metal center are broadened beyond the level of detection.

The ^{1}H NMR spectra of core and core/shell nanoparticles and of the mixture of the surfactants (1:1 mixture of oleic acid and oleylamine) as used in the nanoparticles synthesis are shown in Figure 5. In order to take into account that in the core/shell the surfactant/core/shell is about 1% weight ratio, the amount of core/shell nanoparticles suspended in $CDCl_3$ is ~100 times larger than that of core nanoparticles.

The most notable difference among the three spectra is the remarkable peak broadening and the absence of several peaks in the spectra of the suspended core and core/shell nanoparticles. In the spectrum of the mixture (oleylamine and oleic acid spectra reported in the Supporting Information (SI)), the multiplets present at 2.72 and 2.11 ppm are assigned to the methylene protons of the "f" carbons of the oleic acid and oleylamine, respectively; the multiplet at 5.50 ppm is assigned to the "d" vinylic protons; the multiplet at 1.50 ppm, to the "e" carbons; the multiplet at 1.97 ppm, to "c" carbons external of the vinyl group; the signal at

(30) Geshev, J.; Mikhov, M.; Schmidt, J. E. *J. Appl. Phys.* **1999**, *85*, 7321.
(31) Peddis, D.; Cannas, C.; Musinu, A.; Piccaluga G. *Chem.—Eur. J.* **2009**, 10, *15*(32):7822.
(32) Garcia-Otero, J.; Porto, M.; Rivas, J.; Bunde, A. *J. Appl. Phys.* **1999**, *85*, 2287.
(33) Batle, X.; GArcìa del Muro, M.; Labrta, A. *Phys. Rev. B* **1997**, *55*, 6440.
(34) Osman, M. A.; Seyfang, G.; Suter, U. W. *J. Phys. Chem. B* **2000**, *104*(18), 4433.
(35) Sinclair, R. G.; Mckay, A. F.; Myers, G. S.; Jones, R. N. *J. Am. Chem. Soc.* **1952**, *74*, 2578.
(36) Franzman, M. A.; Perez, W.; Brutchey, R. L. *J. Phys. Chem. C* **2009**, *113*, 630.
(37) La Mar, G. N.; Horrocks, W. D., Jr.; Holm, R. H. *NMR of paramagnetic molecules*; Academic Press: New York, 1973.

1.25 ppm, to the "b" carbons; and the signal at 0.83 ppm, to the "a" methyl group. The "g" signal is ascribed to hydrogen bonding, arising from the acid−base complex of an oleic acid molecule with an oleylamine molecule.

The ^{1}H NMR spectra of the suspended core and core/shell nanoparticles show a broad peak at 0.83 ppm which can be attributed to the methyl group ("a" carbons), a signal at 1.25 ppm which can be attributed to CH_2 groups ("b" carbons) far from the carboxylic, the amine and the vinylic group, and a signal at about 1.6 ppm. This signal is due to the presence of water, which, in chloroform, falls at 1.6 ppm, and is rather narrow in the core/shell nanoparticles and broad in the core nanoparticles. The difference in the broadening of the signal at 1.6 ppm could be ascribable to the fact that in the core/shell sample the water molecules should be far away from the magnetic core due to the presence of the silica shell. Other signals from methylene groups cannot be assigned because they would be superimposed to this signal of water.

The presence of the signals attributed to methyl and methylene groups of the surfactants confirm the presence of the mixture both in the core and core/shell nanoparticles. The disappearance of several characteristic signals, which are ascribable to vinyl groups and CH_2 close to carboxylic and ammine groups, due to line broadening beyond detection caused by the effect of superparamagnetic properties of the cobalt ferrite nanoparticles, confirm the bonding of the surfactants to the nanoparticles.

In order to have more information about the bound of the surfactant with the nanoparticle surface, FTIR spectra were performed.

Figure 6 shows FTIR spectra of core and core/shell nanoparticles and of the mixture, as used in the nanoparticles synthesis. The spectrum of the surfactant mixture (Figure 6a) reveals modes characteristic of the oleyl group:[38] the peaks at 2855 and 2931 cm^{-1} are due to the symmetric and asymmetric CH_2 stretching modes, and the peak at 3006 cm^{-1} is attributed to a cis —HC═CH— arrangement.[39] It is important to observe that the spectrum of the mixture is not a simple combination of the spectra of the pure components' surfactants (SI). The peak at 1706 cm^{-1}, which is typical of the ν(C═O) mode of the COOH group, is very small, and the 3370 cm^{-1} asymmetric stretching, the 3294 cm^{-1} symmetric stretching, and the 1608 cm^{-1} scissoring modes of the NH_2 group are absent. The most obvious explanation for the almost complete absence of these peaks is that the mixture of oleic acid and oleylamine consists of an acid−base complex of —COO^- and —NH_3^+ ions.

This is further confirmed by the presence of modes associated with $\nu_a(COO^-)$ and $\nu_s(COO^-)$ modes of the carboxylate group observed at 1554 and 1394 cm^{-1}.[38] Furthermore, a shoulder is observed at 1622 cm^{-1}, which can be attributed to the antisymmetric deformation of the $-NH_3^+$ group, considering that protonated amines display an antisymmetric deformation in the 1625−1560 cm^{-1} range and a symmetric deformation in the 1550−1505 cm^{-1} range.[40,41] The modes observed in spectrum in the frequency region below 1500 cm^{-1} arise from complex combinations of the ν(C−C) stretch, ν(C−O) stretches, CH_2 deformations, and other motions related to NH_3^+, which are too complex to be assigned. In particular, the spectrum shows an intense peak at 715 cm^{-1} which is typical of the CH_2 rocking modes.

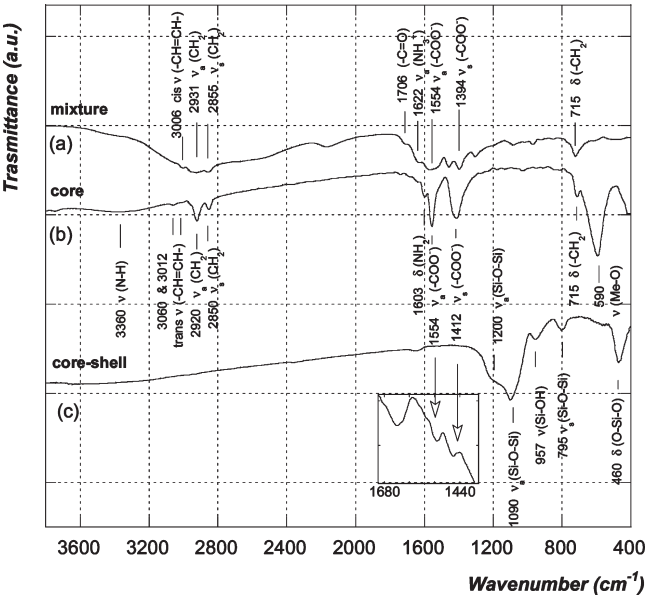

Figure 6. FTIR spectra of (a) core/shell nanoparticles, (b) core, and (c) the mixture of the surfactants (1:1 mixture of oleic acid and oleylamine). (inset) Detail of silica saturated spectrum of core/shell sample.

The spectrum of the core nanoparticles is reported in Figure 6b. Comparison of the FTIR spectra in Figure 6a and b gives several interesting suggestions. Besides the peak at 590 cm^{-1}, ascribed to the Me—O modes in the ferrite nanoparticles, two main peaks are observed at 1554 and 1412 cm^{-1}, indicating the presence of modes associated with $\nu_a(COO^-)$ and $\nu_s(COO^-)$ of the carboxylate group, which, in turn, suggest the presence of bidentate carboxylate bonded to the nanoparticle surface. The spectrum of core nanoparticles also shows modes characteristic of the amine group: a large peak at ~3360 cm^{-1}, which can be attributed to the stretching mode ν(N—H) of the NH_2 group and a peak at 1603 cm^{-1} due to the NH_2 scissoring mode. The presence of these peaks would suggest the presence of pure oleylamine. In the high wavenumber region, FTIR spectroscopy has often been used to probe the conformation and orientation of alkyl chains. The frequency, width, and intensity of the asymmetric $\nu_a(CH_2)$ and symmetric $\nu_s(CH_2)$ methylene stretching bands, near 2920 and 2850 cm^{-1} respectively, were found to be sensitive to the cis/trans conformer ratio.[34,42] Therefore, these vibrational modes can be used to monitor changes in the ordering and packing of the chains. In the spectrum

(38) Shukla, N.; Chao Liu, M.; Jones Dieter Weller, J.M.M.M. **2003**, *206*, 178; and refs therein.
(39) Gasgnier, M. *J. Mater. Sci.* **2001**, *20*, 1259.
(40) Lin-Vien, D.; Colthup, N. B.; Fateley, W. G.; Grasselli, J. G. *The Handbook of Infrared and Raman Characteristic Frequencies in Organic Molecules*; Academic Press: London, 1991.
(41) Lawrie, G.; Keen, I.; Drew, B.; Chandler-Temple, A.; Rintoul, L.; Fredericks, P.; Grøndahl, L. *Biomacromolecules* **2007**, *8*(8), 2533.
(42) Osman, M. A.; Suter, U. W. *Chem. Mater.* **2002**, *14*, 4408.

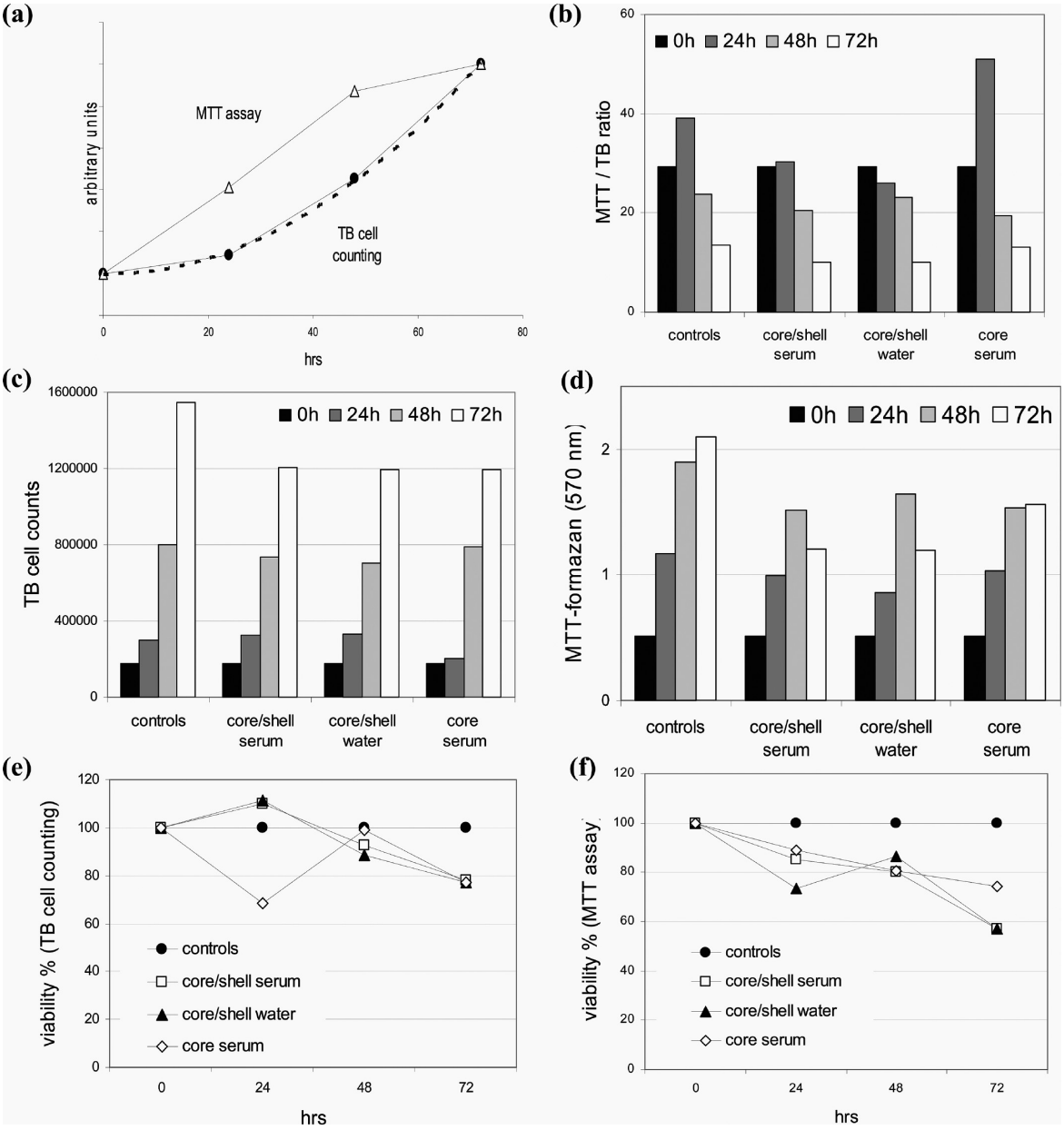

Figure 7. Viability of CEM cells treated with core/shell and core nanoparticles for 24, 48, and 72 h. (a) MTT assay and TB cell counts of control cells at the different time points. The dashed line represents the exponential fitting ($r = 0.994$). (b) MTT/TB ratios at different time points. (c) TB cell counts at different time points. (d) MTT−formazan at different time points. (e) Cell viability based on TB cell counts at different time points. (f) Cell viability based on MTT assay at different time points.

of the core nanoparticles, a narrowing of the $\nu_a(CH_2)$ is observed, which can be associated with a more dense packing of the alkyl chains. This conclusion is also justified by the signals which appeared in this sample from 3000 to 3100 cm^{-1}, a peak at 3060 cm^{-1}, and a small band at ~3012 cm^{-1}, which are consistent to the presence of a trans —HC═CH— arrangement (elaidic form derived from trans-isomer of oleic acid called elaidic acid).[35]

The IR spectrum of core/shell nanoparticles (Figure 6c) exhibits a series of bands which are typical of the vibrational normal modes of silica, while the peak at 590 cm^{-1} is ascribed to the Me—O modes, due to the presence of ferrite nanoparticles. The signals attributed to the surfactant, due to the 1% surfactant/core/shell weight ratio, very hardly can be sorted out in the spectrum. However, collecting a spectrum where the strong silica signal at ~1100 cm^{-1} has been saturated (inset), allows the observation of two signals in the 1450−1530 cm^{-1} range which can be assigned to $\nu_a(COO^-)$ and $\nu_s(COO^-)$ modes of the carboxylate group. These results, in agreement with NMR data, confirm that the surfactant environment remains unchanged also in the silica coated nanoparticles.

Cytotoxicity Tests. *TB Assay*. Direct counting of untreated cells at four time points (0, 24, 48, and 72 h) depicted a typical exponential growth curve ($r = 0.994$) (Figure 7a), consistent with the kinetic proliferation of cells not affected by contact inhibition. Compared to control cells, the number of nanoparticle-treated cells showed irregular fluctuations, especially at 24 h (Figure 7c e). On the basis of the regularity of baseline

data and the progressive convergence of data at the next time points (48 and 72 h), these fluctuations can not be attributed to inaccuracy of data but, rather, to positive or negative interferences of nanoparticles on cell proliferation. After 72 h of treatment, all samples showed a 20% viability loss (Figure 7e).

MTT Assay. In contrast with TB data, control cells stained with MTT showed a linear increase of formazan at 24 and 48 h, followed by a slowdown at 72 h (Figure 7a). This fact suggests that the rate of MTT−formazan production is not purely related to the cell number but may change in different stages of proliferation as a result, for example, of a decreased ability of cells to endocytate MTT. The rate of formazan production at 72 h was still further reduced in cells treated with nanoparticles (Figure 7d). To account for the amount of MTT−formazan produced by a single cell at different time points, we calculated the ratio between MTT−formazan absorbance and TB cell counts (Figure 7b). This value resulted progressively decreased between 24 and 72 h in all (treated and untreated) groups. The lowest MTT/TB ratio was detected in cells treated with core/shell nanoparticles (both in water and serum) for 72 h. Thus, cell viability calculated by the MTT assay (Figure 7f) can be reasonably considered as underestimated.

Discussion and Conclusions

The combination of the high-temperature decomposition of acetylacetonates, in the presence of a mixture of oleic acid and oleylamine, and of a microemulsion method has allowed us to synthesize $CoFe_2O_4$ nanoparticles coated by a silica shell. The ferrite core nanoparticles have a narrow particle size distribution and self-assemble in hexagonal close packing. The core/shell particles also exhibit a narrow distribution, and the majority of shells encompasses a single ferrite (core) nanoparticle. The mean average size of the core is about 8 nm, and the silica shell thickness is about 12−13 nm. Both synthesis methods, either that of the core or that of the shell, are very flexible and useful to synthesize nanocomposites with tunable features in a large range.

The magnetic properties of the core and core/shell nanoparticles are very similar, being the only difference determined by the presence of a silica shell which reduces the value of saturation magnetization and the extent of interparticle interactions. In fact, both samples are superparamagnetic at room temperature and have an identical distribution of magnetic anisotropy, while the variation of the blocking temperatures is the result of differences of the interactions. δM analysis indicates a clear prevalence of dipolar interactions, confirming that nanoparticles aggregation does not occur in both samples.

This behavior suggests that the core nanoparticles derived by the thermal decomposition are coated by a shell of surfactant residual (coming from an oleic acid and oleylamine mixture) and that this shell remains unchanged also in the silica coated nanoparticles. In this way, the magnetic properties of the core (ferrite nanoparticles + surfactant coating) do not undergo a change due to the silica shell, in contrast with the situation occurring in nanocomposites where silica is direct-coupled with the ferritic oxide. This renders the system studied here more attractive in view of the possibility of easily regulating the magnetic properties of the nanocomposite.

The hypothesis reported above is further confirmed by spectroscopic results. The ^{1}H NMR spectra of the two samples exhibits the same signals, due to the $-CH_2$ and $-CH_3$ groups which are far from the superparamagnetic nanoparticles, while the signals of the groups close to the nanoparticles, including those of the vinyl group, become large beyond detection.

The surfactant coating is therefore present in both core and core/shell samples. FTIR results reveal that the surfactant is bonded to the nanoparticles core through carboxyl groups and that the vynil group is still present in the surfactant, contrary to what is reported in other investigations.[20] Moreover, in agreement with other studies, the oleic group undergoes a change into elaidic group when bonded to the nanoparticles' core.[35]

The comparison of cytotoxicity data in the presence of core or silica-coated nanoparticles suggests that silica coating does not affect the cell viability in a significant way.

These results can be explained by two different points of view. Actually, nanoparticles are much smaller than endocytotic vesicles. It may be therefore supposed that both core and core/shell particles, entrapped in serum, are internalized in equal amounts, and this may result in comparable cytotoxic effects. According to this view, if on one hand the presence of serum has the advantage of inhibiting nanoparticle aggregation, on the other hand it may lead to a nonselective import of nanoparticles inside the cell. Moreover, it is well-known that SiO_2 prepared via base catalyzed polycondensation of TEOS is porous favoring percolation of small species like ions or water through a silica shell. These data further confirm that oxide nanoparticles are covered in both samples by a homogeneous protective organic envelopment.

Supporting Information Available: XRD, ^{1}H NMR, and FTIR spectra and details on the cytotoxicity tests. This material is available free of charge via the Internet at http://pubs.acs.org.